CSIRO PUBLISHING
www.publish.csiro.au/journals/eg *Exploration Geophysics*, 2008, **39**, 189–197

Multi-component seismic-resolution analysis using finite-difference acquisition modelling*

Shaun Strong[1,2] Steve Hearn[1,2]

[1]Velseis Pty Ltd and University of Queensland, Brisbane, Australia.
[2]Corresponding authors. Email: sstrong@velseis.com; shearn@velseis.com

Abstract. Various rules-of-thumb (e.g. Fresnel radius, Rayleigh limit) are commonly used to predict seismic resolution, based on the dominant frequency on the image. However, seismic resolution ultimately depends on more fundamental parameters including survey design, source bandwidth, geology, and data processing. A more instructive analysis is possible via numerical modelling of the acquisition process. Here we demonstrate the improved insight available with this approach, using examples taken from the petroleum and coal sectors.

We use viscoelastic finite-difference modelling to simulate 2D multi-component acquisition sequences. The ability to allow for anelastic attenuation is important as it permits a more realistic comparison of the resolution achievable on P-wave and converted-wave (PS) imagery.

An examination of vertical resolution for a wedge model on a petroleum scale indicates that processed P-wave sections have poorer resolution (62 m) than predicted by the Widess (20 m) and Rayleigh (40 m) resolution limits. For this model the vertical resolution for the PS data is comparable to that of the P-wave data. This is in agreement with the theoretical relative-resolution relationship.

A second example examines detection of lens-like features at petroleum depth. The resolving ability on the P-wave imagery is broadly consistent with analytical predictions appropriate to migrated data (100 m laterally and 40 m vertically). Again PS resolution is comparable to P resolution.

Analysis of a typical coal target suggests that barren-zones of width 5–10 m can be resolved. The interplay of wavelength and attenuation is such that the PS image is likely to exhibit comparable, or slightly reduced, lateral resolution, provided statics are not a problem. Resolution can be downgraded significantly if statics are more severe, and in practice this is likely to have greater impact on the PS image.

Realistic numerical modelling, simulating the full acquisition and processing sequence, leads to a more pragmatic understanding of seismic resolution issues. It is a valuable tool for survey planning and image interpretation.

Key words: modelling, multi-component, resolution.

Introduction

Several simple rules-of-thumb have been widely used to predict vertical and horizontal resolution limits (e.g. Rayleigh and Widess limits; Fresnel radius (see e.g. Sheriff, 1999; Lindsey, 1989)). Such indicators have been extended via more recent analytical studies. For example, Chen and Schuster (1999) gave expressions to predict the resolution achievable with migrated data. These measures all provide valuable insight into the relationship between dominant frequency and resolution. However, seismic resolution ultimately depends on more fundamental factors. These include survey design (fold, receiver spacing, aperture etc.), source bandwidth, geology, and the design and sequence of algorithms used in the common-midpoint (CMP) stacking process. As targets become more subtle, resolution analysis needs to be more controllable in terms of these individual factors.

The idea of extending our understanding of resolution via modelling is not new. Hilterman (1982) carried out a range of zero-offset resolution modelling exercises, and increasingly sophisticated schemes have since evolved. For this investigation, we use viscoelastic finite-difference modelling (e.g. Robertsson et al., 1994) to simulate the acquisition of a full set of multi-component shot records over 2D geological models of arbitrary complexity. The shooting sequence and geometry is based on realistic CMP-style acquisition parameters. We will use the term *acquisition modelling* to describe this numerical simulation of the acquisition process. The output shot records are analogous to those acquired in a real survey and can be processed and interpreted using standard real-data methods. This provides the ability to compare different processing algorithms with respect to resolution. Figure 1 gives a general outline of the modelling and processing steps used in this investigation.

An advantage of viscoelastic finite-difference modelling is that it incorporates independent attenuation parameters for P and S waves (viz. Q_P, Q_S). This allows instructive examination of the competing effects of shorter wavelength, but increased attenuation, for S waves, and permits comparison of the resolution capabilities of conventional and converted-wave (PS-wave) images.

Analytical comparison of P and PS resolution

As background for the interpretation of our modelled images, we first examine some fundamental theoretical relationships between P and PS resolution.

*Presented at the 19th ASEG Geophysical Conference & Exhibition, November 2007.

 10.1071/EG08023 0812-3985/08/040189

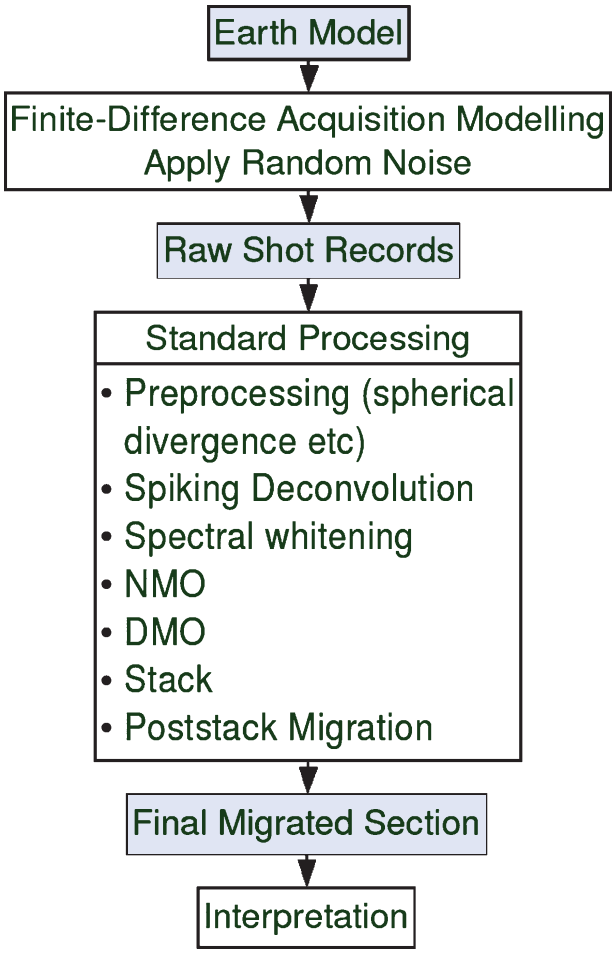

Fig. 1. Outline of the modelling and processing procedures used in this resolution analysis.

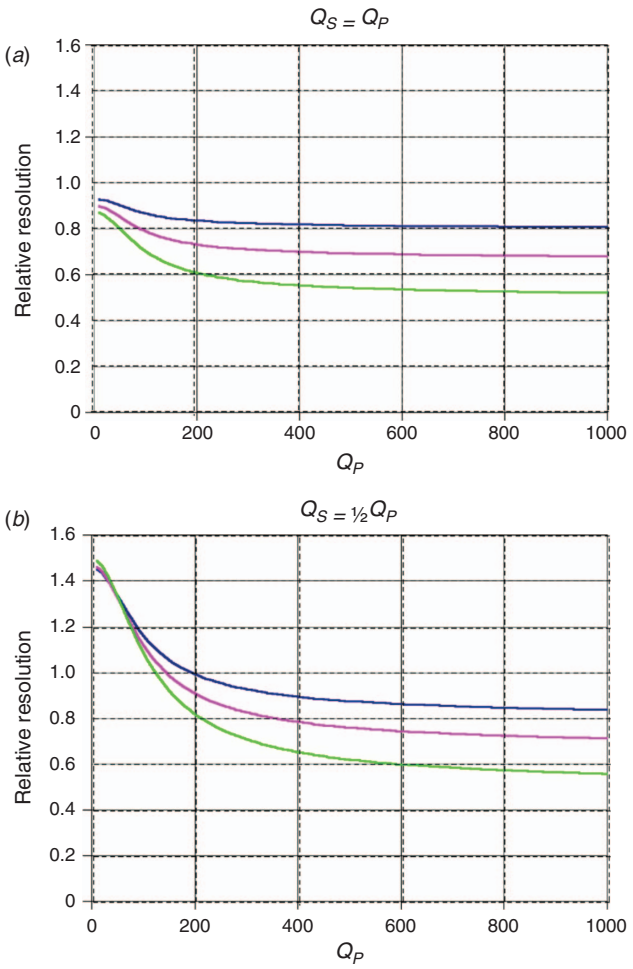

Fig. 2. Analytical comparison of P and PS resolution limits. A value less than 1 implies the PS resolution is better than the P resolution. Figures generated using typical petroleum scale parameters (depth 1750 m; offset of 1750 m) and using equations (1) and (2). (*a*) model with $Q_S = Q_P$; (*b*) $Q_S = Q_P/2$. Resolution limit curves are calculated for several V_P/V_S values: $V_P/V_S = 1.5$ (navy); $V_P/V_S = 2.0$ (magenta); and $V_P/V_S = 3.0$ (green).

Most previous analyses of seismic resolution have been restricted to P-wave imagery, with the standard analytical measures of resolution being related to P-wave dominant frequency (or wavelength). With increasing interest in PS reflection seismology, it is timely to extend resolution analysis to include both P and PS imagery.

The term resolution limit is commonly used to define the smallest vertical separation (δz), for which two reflection interfaces can be resolved. It can be shown (Appendix) that the resolution limits on the P and PS images (δz_P and δz_{PS} respectively) are related via

$$\frac{\delta z_{PS}}{\delta z_P} = \frac{f_P}{f_{PS}} \frac{2}{(1 + V_P/V_S)}. \quad (1)$$

Here f_P and f_{PS} are the dominant frequencies on the P and PS images, respectively, and V_P and V_S are the P- and S-wave velocities, respectively, in the zone of interest. For typical environments the V_P/V_S ratio is often ~2. Hence if the dominant frequencies on the two images were similar, the resolution limit on the PS image would be ~2/3 that on the P image. That is, we would expect PS resolution to be significantly better than P resolution. This proposition was arguably one catalyst for early efforts in converted-wave reflection.

However, working against this is the effect of anelasticity. The dominant frequencies on the P and PS images are influenced differently by the anelastic attenuation suffered along the ray path. This attenuation increases with frequency, according to

$$A(f) = \exp(-\pi T f/Q). \quad (2)$$

Here T is the travel time along a path segment having quality factor Q. The travel time (T) will always be greater for the PS reflection than for the P reflection. That is, the higher frequencies are attenuated more rapidly, resulting in lower dominant frequency on the PS image. This reduces the resolution advantage, according to equation (1).

These two competing effects are illustrated graphically in Figure 2*a*, for a typical petroleum-scale model. A Ricker wavelet has been attenuated according to equation (2), based on paths appropriate to P and PS reflections for the defined target. The resultant dominant frequencies (f_P and f_{PS}) are then used in equation (1) to obtain the relative resolution. A value of 1 on the vertical axis means identical resolution, and values less than one mean PS resolution is better.

For high Q values (to the right) the attenuation effect is less important and hence the PS image has better relative resolution. For a typical V_P/V_S ratio of 2 (Figure 2*a*, magenta) the relative resolution approaches 2/3 for high Q values in accordance

with our early analysis of equation (1). For low Q situations (to the left) the attenuation effect becomes stronger and reduces the advantage of PS imaging.

This analysis assumes the same Q value for P and S waves, and predicts that PS resolution should always be better than for P. This changes if Q_P and Q_S are different. For example, if Q_S is half Q_P (Figure 2*b*) then the resolution advantage is lost for practical Q values (say, $Q_P < 200$).

The preceding analysis has been presented to indicate theoretical resolution comparisons for PS and P images for a very simplistic case. For more realistic structures (e.g. spatially varying V_P/V_S and Q_P/Q_S ratios) this analytical approach is more difficult to use. As seen below, viscoelastic modelling is better suited to such analysis.

Petroleum-scale modelling examples

Wedge model

To demonstrate fundamental resolution results for P and PS images at petroleum depths, we examine the classical wedge model (Figure 3*a*). This type of model has been well documented (e.g. Widess, 1973; Okaya, 1995) and is generally considered a good indicator of vertical resolution issues. For this initial examination we have used a 2-layer Q model and have assumed that Q_P and Q_S are the same, a reasonable starting assumption (e.g. Toksöz et al., 1979).

On each of the seismic images in Figure 3 we have indicated our interpreted resolution limit (red arrow). The corresponding numerical values are given in the caption. For the purposes of this paper we use a pragmatic definition of the resolution limit, as the thickness at which one or both of the main reflection events are distorted to the extent that the interpretation is compromised.

For reference, Table 1 (rows 2–4) gives the classical analytical indicators (Rayleigh resolution limit, $\lambda/4$; Widess limit, $\lambda/8$; detectable limit, $\lambda/30$) for the wedge model at petroleum depth. Table 1 (rows 5–6) also gives the relative resolution (PS to P) based on equation (1), for two cases: $f_{PS}=f_P$, and $f_{PS}=f_P/2$.

The P-wave image in Figure 3*b* is produced with classical zero-offset modelling, and the interpreted resolution limit is in reasonable agreement with the Rayleigh resolution limit given in Table 1. Figure 3*c* has been produced with the more realistic acquisition-modelling approach, but assumes an elastic earth. The reality of CMP processing degrades resolution compared to the zero-offset case. The P-wave image in Figure 3*d* also incorporates anelasticity. In this case the resolution is not degraded much compared to the elastic case.

Figure 3*e* shows the PS image derived with full acquisition modelling, but assuming an elastic earth. The resolution is superior to the comparable P-wave image (Figure 3*c*). However, when the effects of anelasticity are allowed for, the PS image is much more significantly degraded (Figure 3*f*). In this situation, the P and PS images exhibit comparable resolutions (Figures 3*c*, 3*f*).

The effects of anelastic attenuation can be further clarified in terms of dominant frequencies (Figure 4). In the anelastic P spectrum (red) the high frequencies are attenuated compared to the source spectrum (green), but the dominant frequency is only slightly reduced. This explains why the interpreted resolution limits are very similar for the elastic and anelastic cases (Figures 3*c*, 3*d*). On the other hand, the anelastic PS spectrum (blue) is highly attenuated resulting in a significant reduction in the dominant frequency and consequent loss of resolution (Figure 3*f*) relative to the elastic case (Figure 3*e*). Finally, note that the dominant frequencies on the anelastic P and PS spectra are related via $f_P \sim 1.4\, f_{PS}$. Substitution into equation (1), and using the model V_P/V_S of 1.8, yields a relative resolution of unity as observed on the seismic images.

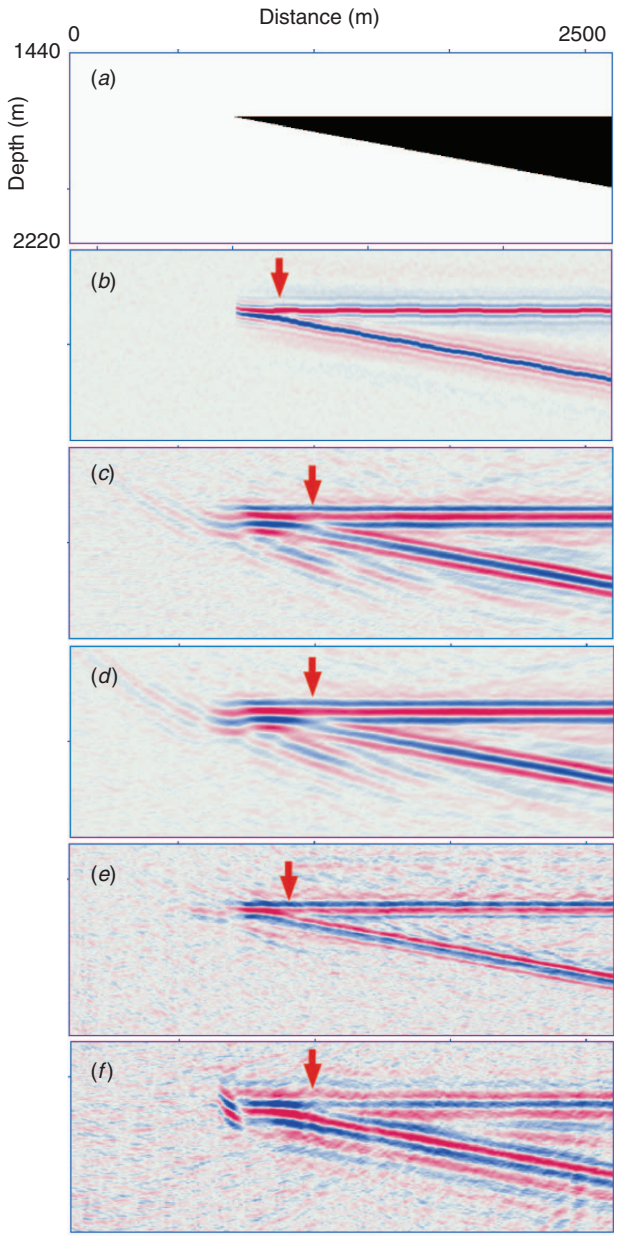

Fig. 3. (*a*) Petroleum-scale wedge model. The top of the wedge is at a depth of 1700 m and the bottom has a 9-degree dip. The wedge has a density of 2700 kg/m^3, P-wave velocity of 4000 m/s and S-wave velocity of 2200 m/s. The country rock has a density of 2500 kg/m^3, P-wave velocity of 3750 m/s and S-wave velocity of 1560 m/s. The Q model comprises a weathering Q value of 10 that penetrates to a depth of 15 m and second layer with a Q value of 100 that extends to the bottom of the model. We have used Q values that are slightly lower than expected to partially allow for the real-life effects of scattering. (*b*) P-wave, zero-offset modelling. (*c–f*) full acquisition modelling: (*c*) P-wave (elastic); (*d*) P-wave (anelastic); (*e*) PS (elastic); (*f*) PS (anelastic). All images have been scaled such that they represent the depth extent marked on the model. The interpreted resolution limits (shown by the red arrows) are: (*b*) 41 m, (*c*) 62 m, (*d*) 62 m, (*e*) 45 m, (*f*) 62 m.

Table 1. Analytical indicators of vertical resolution for a petroleum target at a depth of 1700 m. The assumed wavelength (160 m) has been estimated from the modelled data for this example. The final two rows give relative resolutions for the cases where the dominant frequency on the PS image is equal to, and half of, the dominant frequency on the P image, respectively.

	Resolution (m)
P wavelength	160
Rayleigh resolution limit ($\lambda/4$)	40
Widess limit ($\lambda/8$)	20
Detectable limit ($\lambda/30$)	5
Relative resolution ($f_{PS}=f_P$)	0.7
Relative resolution ($f_{PS}=f_P/2$)	1.4

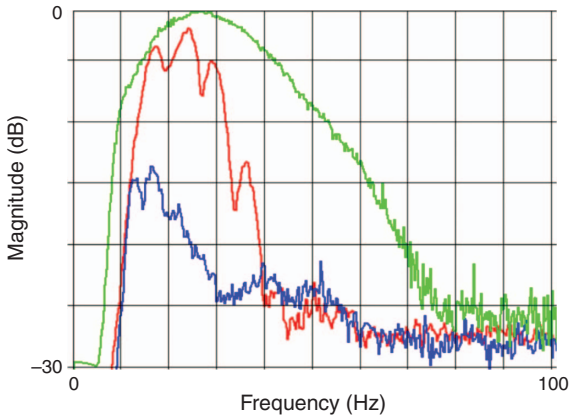

Fig. 4. Magnitude spectra corresponding to the anelastic models in Figures 3*d* and 3*f*. The high frequencies of P and PS spectra (red and blue, respectively) have been attenuated compared to the source (green). The lower magnitude on the PS spectrum compared to the P spectrum is consistent with the lower signal-to-noise ratio of the PS image. The dominant frequency on the P spectrum is ~1.4 times that on the PS spectrum leading to a comparable resolution on the P and PS images (Figure 3).

As indicated above, viscoelastic modelling produces records analogous to raw field data, which can be processed using standard production techniques. The choice of processing flow, and parameters, can influence the resolution on the final seismic image. As a simple example, Figure 5 illustrates that converted-wave dip moveout (DMO) is essential to achieving a high resolution PS image. We see that removal of this algorithm from the processing flow reduces the vertical resolution of the data (from 62 m to 76 m). This suggests that viscoelastic modelling can be used to tweak the processing flow to provide improved resolution of real data.

Lens model

As a second example of resolution analysis at the petroleum scale we consider a model (Figure 6*a*) comprising sand lenses of various sizes and having the same velocity and density properties as the wedge model. A model of this type allows us to confirm vertical resolution results demonstrated by the wedge model. It also allows us to examine horizontal resolution by considering how well the different sized lenses are imaged.

Figures 6*b* and 6*c* show the P and PS images produced for the lens model. A close examination of these figures shows that for the P image the vertical resolution limit is between 50 and 60 m. This is again poorer than the Rayleigh resolution limit (40 m) and on the same order as the wedge model (62 m).

The lens model can also be used to illustrate lateral resolution issues. Lateral resolution of unmigrated data is generally

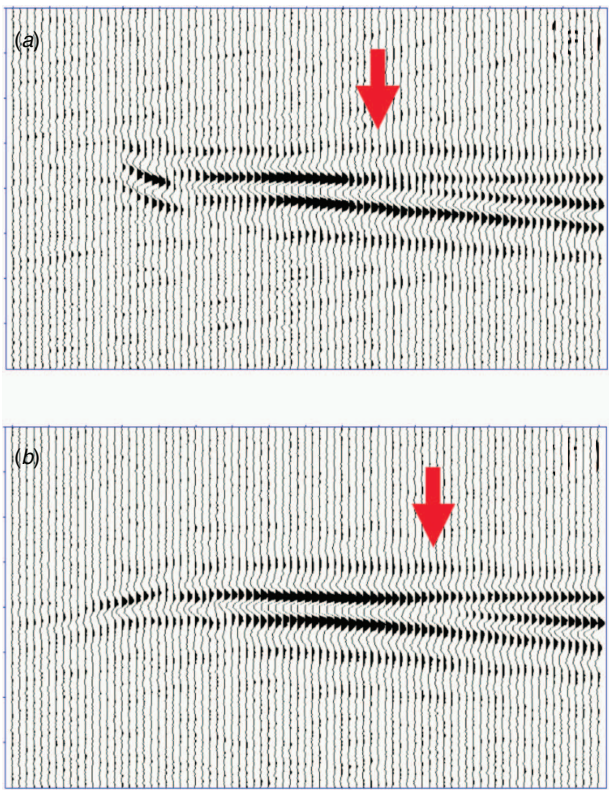

Fig. 5. Effect of processing flow on PS image resolution. (*a*) DMO included in processing flow: resolution limit = 62 m, (*b*) No DMO included in processing flow: resolution limit = 76 m.

considered to be related to the size of the Fresnel zone. The Fresnel zone radii (r) for P and PS waves can be easily calculated for the case of a single layer homogeneous earth using equation (3) (Sheriff, 1999) and equation (4) (Eaton et al., 1991), respectively.

$$r_P = \sqrt{\frac{V_P Z}{2 f_P}} \tag{3}$$

$$r_{PS} = \sqrt{\frac{V_P Z}{(1 + V_P/V_S) f_{PS}}} \tag{4}$$

V_P and V_S are the P and S-wave velocities, f_P and f_{PS} are the dominant frequencies of the P and PS images and Z is the depth of the target.

Because we generally use migrated data for interpretation, another simple expression (equation 5) has been suggested by Chen and Schuster (1999) to better estimate the horizontal resolution (Δx) of migrated P-wave images.

$$\Delta x = Z\lambda_P / L, \tag{5}$$

where Z is the depth of the target, λ_P is the dominant wavelength of the recorded P-wave, and L is the migration aperture.

Table 2 shows the predicted analytical resolution values for the lens model.

Close examination of the P-wave image (Figure 6*b*) suggests that the lateral character of the lens can still be defined for the 100 m body but not the smaller ones. That is, the P-wave horizontal resolution limit is less than 100 m. This indicates that the horizontal resolution is significantly better than the Fresnel radius (370 m) as expected because we are examining

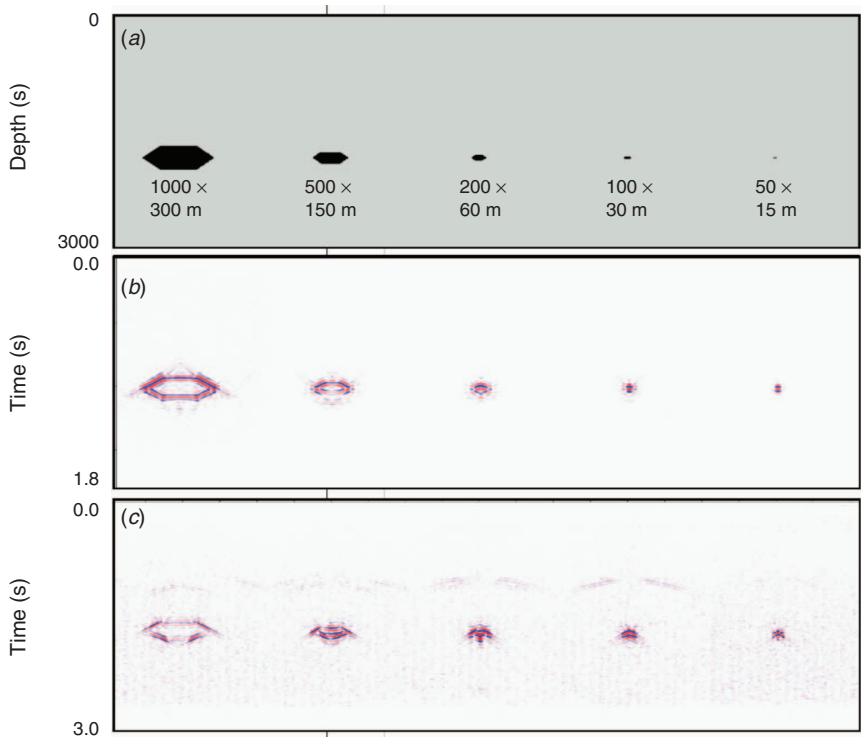

Fig. 6. Lens model. (*a*) The model has the same properties as the wedge model and includes lenses ranging in size from 1000 × 300 m to 50 × 15 m; (*b*) P image; (*c*) PS image.

Table 2. Analytical indicators of lateral resolution for petroleum targets at different depths. All values are in metres. The row printed in bold (1850 m) corresponds to the target depth in Figure 6. The Fresnel radii are appropriate to unmigrated data. The final column gives estimates predicted by Chen and Schuster (1999) for migrated P images.

Depth	P Fresnel radius	PS Fresnel radius		Approximate P resolution after migration (Chen and Schuster 1999)
		$f_{PS}=f_P$	$f_{PS}=f_P/2$	
1600	344	268	379	79
1850	**370**	**288**	**407**	**91**
2100	394	307	434	104
2350	417	325	459	116

migrated data. The Chen and Schuster approximation for migrated data predicts a resolution limit of 90 m for this model, in agreement with our modelled results. A detailed examination of the PS images indicates that the horizontal and vertical resolution is no better than that of the P images and reiterates that the potential advantages of using PS imaging for increased resolution can be negated by reduced bandwidth due to attenuation and more difficult processing.

Coal-scale modelling example

For our third example we examine lateral resolution in a coal-scale environment. Table 3 presents analytical indicators of lateral resolution for coal-scale targets at different depths. As an example, we will consider the target at 150 m depth in some detail. Columns 2–4 give Fresnel radii for P waves, and for PS waves under different frequency assumptions. Because these numbers can be considered indicative of lateral resolution on

Table 3. Analytical indicators of lateral resolution for coal targets at different depths. All values are in metres. The row printed in bold (150 m) corresponds to the target depth in Figure 7. The Fresnel radii are appropriate to unmigrated data. The final column gives estimates predicted by Chen and Schuster (1999) for migrated P images.

Depth	P Fresnel radius	PS Fresnel radius		Approximate P resolution after migration (Chen and Schuster 1999)
		$f_{PS}=f_P$	$f_{PS}=f_P/2$	
50	34	26	37	4
100	48	37	53	8
150	**59**	**46**	**65**	**12**
200	68	53	75	15
250	76	59	84	19

unmigrated data, they have been used primarily to assess the relative resolution of P and PS data. If the dominant frequencies on P and PS images were comparable, equations (3) and (4) would imply better lateral resolution on a PS image (Fresnel radius = 46 m) than on a P image (Fresnel radius = 59 m). However, our experience with PS coal reflection data suggests that the dominant frequency on the PS image may often be only half that on the P image. On this practical assumption (Table 3, column 4), the Fresnel radius (65 m) would imply slightly reduced resolving power for PS compared to P. The analysis of Chen and Schuster (1999) predicts that the expected resolution on the migrated P-wave image would be ~12 m, and by extension therefore slightly greater on the PS image.

As was demonstrated for the petroleum example, acquisition modelling provides the opportunity to explore the validity of these analytical predictors, and to gain deeper insight regarding underlying causal influences on resolution. We will illustrate the concept with reference to a target coal seam interrupted by so-called barren zones of various widths (Figure 7). In the initial exercise, we have used a Q model where Q_P and Q_S have been made equal throughout the model.

To examine the influence of statics, the modelling process has been carried out for a model with constant weathering profile (25 m thick), and for the same model but with a variable weathering profile (9–38 m thick as shown in Figure 7), which has been extracted from real data. Figures 8*a* and 8*b* show the P and PS images for the constant weathering case. A cursory examination of the P image shows that the wider barren zones on the right are easy to identify. However, it is quite difficult to see the smaller ones on the left. Examination of the corresponding PS image shows that it has similar horizontal resolution to that of the P image. Figures 8*c* and 8*d* show the P and PS images for the variable weathering case with no statics correction. For these sections we see that the PS image appears to be degraded more than the P-wave section, especially where the variation in the weathering layer is the greatest (red arrow).

The images in Figure 8 are instructive in a qualitative sense. However we would like to obtain a more quantitative comparison. For this model, a useful means of assessing lateral resolution is via a simple amplitude attribute, derived over the target coal seam. Figure 9 summarises this attribute for the P and PS images for constant and variable weathering profiles. In these plots the barren zones are associated with a reduction in the relative amplitude.

For the constant weathering case, the amplitude attribute of the P-image (Figure 9, red) can easily detect the barren zone of width

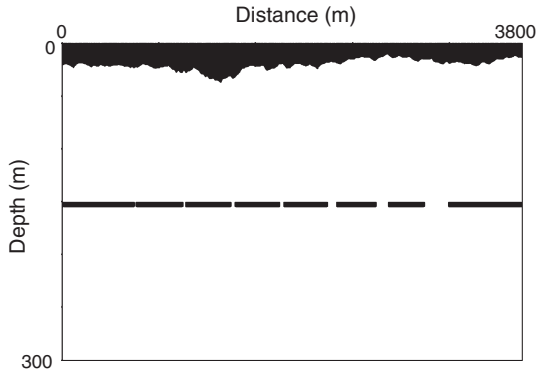

Fig. 7. Coal scale model. The coal seam is at 150 m. It has a thickness of 5 m, density of 1400 kg/m^2, P-wave velocity of 2250 m/s and S-wave velocity of 900 m/s. The coal seam is interrupted by barren zones ranging in width from 5 to 120 m. The country rock has a density of 2500 kg/m^2, P-wave velocity of 4000 m/s and S-wave velocity of 2000 m/s. In the weathering $Q_P = Q_S = 30$ and in the subweathering $Q_P = Q_S = 100$. The model shown here incorporates a laterally varying weathering layer. A constant weathering case has also been considered.

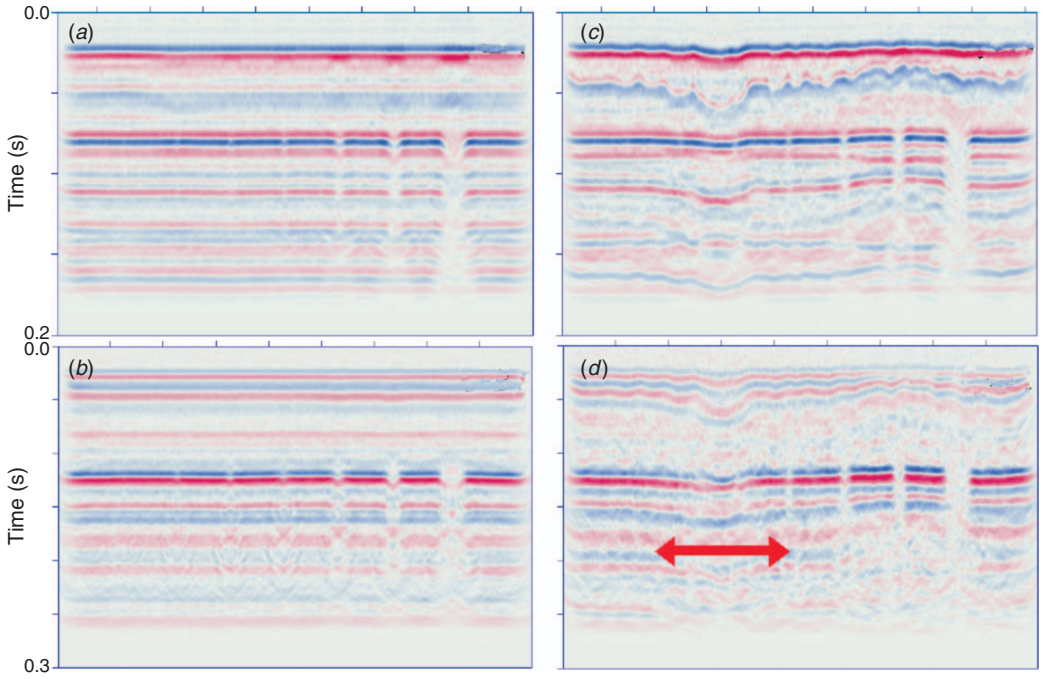

Fig. 8. Seismic sections corresponding to the barren-zone model in Figure 7. (*a*) Constant-weathering P-image; (*b*) constant-weathering PS-image; (*c*) variable-weathering P-image; (*d*) variable-weathering PS-image. The target seam is at ~0.08 s on the P images, and ~0.12 s on the PS images. (Long-period multiples at later times do not influence the resolution analysis on the main event, and have not been specifically attacked in this simple processing flow). The red arrow indicates a zone of reduced data quality associated with greater variation in the weathering layer.

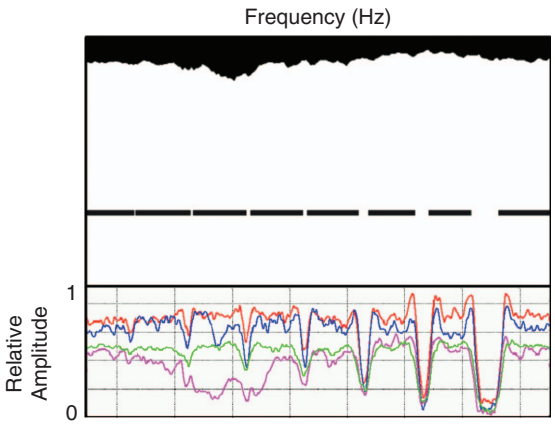

Fig. 9. Amplitude attribute computed for a 40 ms window over the target coal seam. The four curves correspond to the four images in Figure 8. Red: constant-weathering P-image; green: constant-weathering PS-image; blue: variable-weathering P-image; magenta: variable-weathering PS-image.

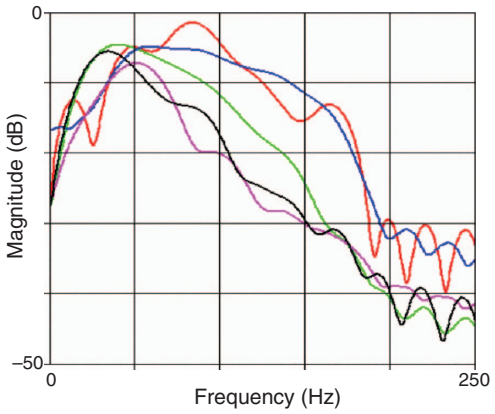

Fig. 10. Coal-scale model: Representative magnitude spectra. Red: constant-weathering P-image; green: constant-weathering PS-image; blue: variable-weathering P-image; magenta: variable-weathering PS-image; black: constant-weathering PS-image for the case where $Q_S = 2/3\ Q_P$.

10 m (second from the left), and can arguably detect the 5 m feature (leftmost). This is significantly better than the Fresnel radius of 60 m and is in agreement with the Chen and Schuster (1999) prediction of 12 m. The amplitude attribute for the corresponding PS image (green) shows that the resolution is arguably slightly poorer than the P image, with an interpreted resolution limit of 10 m.

The amplitude attribute response for the variable-weathering P-image (blue) is slightly noisier and introduces spurious attribute variations of similar scale to the geological features. These can make it more difficult to uniquely identify the smallest barren zones. The magenta curve shows that the PS image is a lot more susceptible to variations in the weathering layer. This has the potential to dramatically reduce the resolution of the PS image.

These broad conclusions regarding lateral resolution are consistent with observed changes in spectral bandwidth over the target horizon. Figure 10 illustrates that the P-wave images for a constant (red) and variable (blue) weathering layer exhibit similar bandwidths. (The slight increase in spectral character for the constant case (red) relates to the spectral periodicity introduced when the base-of-seam reflector is better defined.)

These spectra provide additional insight into the interplay between S wavelength and anelastic attenuation, in controlling the relative resolution on the PS image. First, consider the case

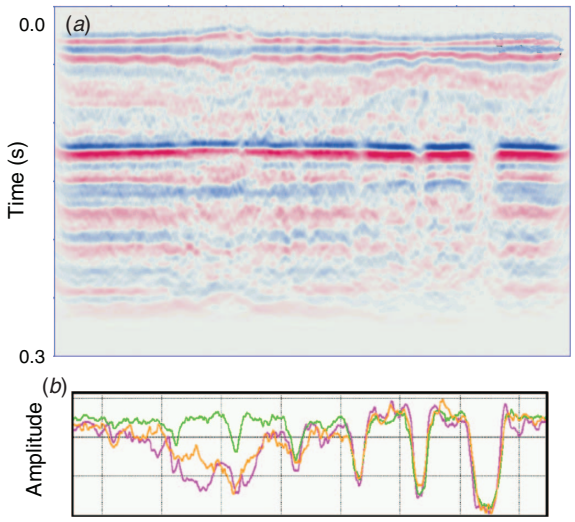

Fig. 11. (*a*) PS image obtained after application of 'ideal' static corrections derived using the known coal-scale model of Figure 7. The image has been improved relative to the uncorrected case (Figure 8*d*) but has reduced signal-to-noise compared to the constant-weathering case (Figure 8*b*). (*b*) Amplitude attribute (orange) corresponding to the statics-corrected PS image in (*a*), compared to those for the uncorrected case (magenta) and the constant-weathering case (green).

where the weathering is constant and where $Q_P = Q_S$ throughout the model. In this situation, the PS spectrum (green) exhibits slightly reduced dominant frequency, and bandwidth, compared to the P-wave spectrum (red). Even though Q values are the same, the PS-waves suffer higher attenuation because the path contains more cycles than for P. This effect is sufficient to cancel the potential resolution advantage attached to the lower velocity (and hence shorter wavelength) of S-waves.

The spectra also emphasise the potentially damaging effects of a variable weathering layer (magenta curve) on PS resolution. Statics reduce the coherency in the stack, and the effect on bandwidth is significant. For example, in the absence of statics, all Q_S values would need to be reduced to 2/3 Q_P to produce a similar bandwidth reduction (black).

These results have been presented without the application of any statics correction to demonstrate relative behaviours. P-wave static correction techniques are very robust and have been proven to provide good results. Therefore the constant weathering case is more analogous to real P-wave data. Note, however, that PS-wave near-surface solutions are more complicated (e.g. Meulenbroek and Hearn, 2007) and therefore the PS results have more potential to vary from the constant weathering case.

Finally, it is noted that the influence of the weathering layer might extend beyond static errors, as demonstrated here for the PS data. The image in Figure 11*a* has been derived by applying pre-stack static corrections based on the known weathering model. That is, it simulates the image obtained with a perfect PS static solution. The image is much improved relative to the case where no static corrections have been applied (Figure 8*d*). However, the signal-to-noise ratio is still poorer than that obtained with the constant weathering model (Figure 8*b*). This relativity is quantified in the three amplitude curves shown in Figure 11*b*. An examination of shot records derived for the variable-weathering model has indicated that the surface-wave noise is much stronger in places where the shot point is not far below the base of weathering (i.e. weathering layer is thicker). This has led to a reduction of the signal-to-noise ratio on the resultant stack and explains the residual amplitude anomalies.

Conclusions

An analysis of P-wave images has indicated that while the Rayleigh resolution limit is appropriate for simple zero-offset models, it is often an overly optimistic estimation of vertical resolution on realistic processed sections. An examination of horizontal resolution has shown that the resolution limit for migrated data can be as low as 1/5 of the Fresnel radius. This is often comparable to the rule of thumb presented by Chen and Schuster (1999).

Analytical comparison of P and PS resolution suggests that in some conditions PS images may have potential for better resolution. However, our full acquisition modelling results have indicated that even with optimal processing, and assuming Q_P and Q_S are similar, P and PS resolutions would be more typically comparable. We have also demonstrated that the complexities of PS statics can further degrade the resolution of PS images. Broadly speaking, these results are consistent with the resolution properties of real data acquired in similar environments (Velseis, 2006).

Acquisition modelling is computationally expensive compared to zero-offset modelling. However, this examination has demonstrated that it leads to a much more realistic assessment of seismic resolution. It is a valuable tool for survey planning and provides increased confidence in real data interpretation.

Acknowledgments

This research makes use of the processing framework provided by Seismic Unix from Colorado School of Mines. We thank Randall Taylor and Binzhong Zhou for constructive reviews, and Lindsay Thomas for editorial suggestions.

References

Chen, J., and Schuster, G. T., 1999, Resolution limits of migrated images: *Geophysics*, **64**, 1046–1053. doi: 10.1190/1.1444612

Eaton, D. W. S., Stewart, R. R., and Harrison, M. P., 1991, The Fresnel zone for P-SV waves: *Geophysics*, **56**, 360–364. doi: 10.1190/1.1443050

Hilterman, F. J., 1982, Interpretive lessons from three-dimensional modeling: *Geophysics*, **47**, 784–808. doi: 10.1190/1.1441347

Lindsey, J. P., 1989, The Fresnel zone and its interpretive significance: *Geophysics: The Leading Edge of Exploration*, **8**, 33–39. doi: 10.1190/1.1439575

Meulenbroek, A., and Hearn, S., 2007, Analysis of converted refractions for shear statics. 19th ASEG Conference, Perth.

Okaya, D. A., 1995, Spectral properties of the earth's contribution to seismic resolution: *Geophysics*, **60**, 241–251. doi: 10.1190/1.1443752

Robertsson, J., Blanch, J., and Symes, W., 1994, Viscoelastic finite-difference modelling: *Geophysics*, **59**, 1444–1456. doi: 10.1190/1.1443701

Sheriff, R. E., 1999, Encyclopedic Dictionary of Exploration Geophysics 3rd edition. Oklahoma.

Toksöz, M. N., Johnston, D. H., and Timur, A., 1979, Attenuation of seismic waves in dry and saturated rocks: 1. Laboratory measurements: *Geophysics*, **44**, 681–690. doi: 10.1190/1.1440969

Velseis 2003, Investigation of converted-wave seismic reflection for improved resolution of coal structures: Final Report: Australian Coal Association Research Program (ACARP) Project C10020.

Velseis 2006, Integrated P-wave/PS-wave seismic imaging for improved geological characterisation of coal environments: Final Report: Australian Coal Association Research Program (ACARP) Project C13029.

Widess, M. B., 1973, How thin is a thin bed? *Geophysics*, **38**, 1176–1180. doi: 10.1190/1.1440403

Manuscript received 7 April 2008; revised manuscript received 1 December 2008.

Appendix

Relative resolution for P and PS reflection

Consider the problem of resolving two interfaces on a conventional P-wave image, where the dominant frequency is f_P. Suppose that a wavelet of this dominant frequency can just resolve two interfaces separated in time by δt_P. On the corresponding PS (converted-wave) image, the dominant frequency will in general be different (say f_{PS}). Resolution in time is directly related to the dominant frequency of the wavelet on the image. Hence the PS wavelet will be able to resolve two interfaces separated in time by

$$\delta t_{PS} = \delta t_P (f_P / f_{PS}). \tag{A1}$$

On the P image, the time-resolution limit (δt_P) corresponds to a depth-resolution limit of

$$\delta z_P = V_P \delta t_P / 2, \tag{A2}$$

where V_P is the P-wave velocity at the zone of interest. On the PS image, the time-depth relationship needs to allow for the fact that the downgoing ray is P and the upgoing ray is S. That is, the time and depth resolution limits would be related by

$$\delta t_{PS} = \delta z_{PS} / V_P + \delta z_{PS} / V_S, \tag{A3}$$

or

$$\delta z_{PS} = \delta t_{PS} V_P / (1 + V_P / V_S), \tag{A4}$$

where V_P and V_S are the P-wave and S-wave velocities in the zone of interest.

By considering equations (A1), (A2), and (A4) we can define the relative resolution as

$$\frac{\delta z_{PS}}{\delta z_P} = \frac{f_P}{f_{PS}} \frac{2}{(1 + V_P / V_S)}. \tag{A5}$$

A ratio less than unity implies that the PS image has better resolution, and vice versa. Velseis (2003) provides additional comment on this topic, including practical examples.